2019 IEEE/RSJ International Conference on Intelligent Robots and Systems (IROS)
Macau, China, November 4-8, 2019

Adaptive Vision-Based Control for Rope-Climbing Robot Manipulator

Guangli Sun, Xiang Li, Peng Li, Linzhu Yue, Zhen Yu, Yang Zhou, Yun-Hui Liu

Abstract— **While the mechanism of Rope-Climbing provides much flexibility, it opens up challenges to the development of the controller for Robotic Manipulator installed on Rope-Climbing robot(*RCR*), which is called *Rope-Climbing Robot Manipulator(RCRM)* here. In particular, the deformable nature of the rope results in the vibration to the manipulator and hence affects the positioning of the end effector. In this paper, a new adaptive vision-based controller is proposed for *RCRM*, which enables the robot to carry out the high-accuracy task under the unknown vibration from the rope. The proposed controller guarantees the performance of the robot in twofold. First, the control problem is directly formulated in the image space such that the exact spatial relationship between the moving base of the manipulator (due to the vibrating rope) and the target (e.g. the wall) is not required. Second, novel adaptation laws are developed to estimate the vibration from the rope online and are cancelled out in the robot control input to stabilize the end effector. The stability of the closed-loop system is rigorously proved with Lyapunov methods, and experimental results are presented to illustrate the performance of the proposed controller.**

I. Introduction

Applications of Rope-Climbing robot(*RCR*) can be found in various areas, such as live power lines maintenance, ROBTET [1], high-rise window cleaning [2] and inspecting suspension bridge hanger rope [3]. High-rise works like cleaning, maintenance, and aloft inspection are complicated and labor-intensive, what's more, dangerous. Comparing with the common automation robots for high-rise works, including pillar-climbing robots [4]–[6], wall-climbing robots [7]–[9], *RCR* can provide more flexibility because it can be deployed everywhere simply just by setting up some wires or ropes [10]. The ability of *RCR* is limited by the manipulator installed on it. If the general robotic arm like universal robotic arm or else mature robotic arm can be served as a general manipulator, the good adaption of *RCR* and the functionality of robotic arm can be combined with to develop a general platform. This general platform will make the high-rise work more efficient, safer and preciser.

A robotic manipulator installed on *RCR*, is called Rope-Climbing Robot Manipulator(*RCRM*). It is a kind of floating-base robotic manipulator. The existing researches for the floating-base robotic manipulator include space robotic manipulator [11], mobile robotic manipulators, under-water robotic manipulators. The base of those manipulators, which are space satellite, mobile cars, underwater vehicles, can be actively controlled. As for the dynamic control of those robots, in the space robotic manipulator system, the moment conservation [12] is an important assumption in its dynamic control. Two flexible arms collaborative control in the rigid spacecraft has been introduced in [13]; in the underwater robotic manipulator system, the adaptive control has been utilized to estimate the dynamic parameters in the dynamic model to handle the time-varying environment [14]; in the mobile robotic manipulator system, the robot base movement has been estimated by a *KF* (Kalman Filter), and compensated in the end effector, adding the environment stiffness estimated by an *EKF* (Extended Kalman Filter), force tracking of the mounted light-weight manipulators has been realized [15]. In a kind of marco-minor robotic manipulator system, the controller utilize inertial force of the small robot to compensate the large arm vibration in [16]. Besides, vision servo has been used in [17] and [18], no attitude control are used in their controller, but the trajectory tracking performance can be guaranteed in their work, which provide us a good direction for floating system control.

Comparing with the refered floating-based robots under vibrating, vibration to the Rope-Climbing Robot Manipulator is limited by rope, so that the robotic arm end effector position can be controlled through itself adjustment without synchronous regulation of the robot base, which makes the whole system simple, cost saving and general.

This paper presents a novel Rope-Climbing Robot Manipulator which provides a platform for different kinds of high-rise work. Then, a new adaptive vision-based controller is proposed for the *RCRM*, which enables the robot to carry out the high-accuracy task subject to the unknown vibration from the rope. The stability of the closed-loop system is rigorously proved with Lyapunov methods, and experimental results are presented to illustrate the performance of the proposed controller.

II. Problem Formation

The *RCRM* is combined with four parts as shown in Fig. 1: the stainless rope, the rope climbing robot, the robotic arm, and the end effector (i.e. a cleaning mop with a web camera). The *RCR* is installed on three steel ropes, and the robotic arm, is installed at the bottom of *RCR*. The detail mechanical principle of *RCR* can be seen in our previous work [19]. The sensors in the systems are an IMU, a camera, and robotic arm embedded sensors. Data from the IMU includes base position, velocity and acceleration, the camera installed at the end of the robotic arm can detect the feature point of the

G. Sun, L. Yue, Y. Zhou, and Y.-H. Liu are with the Department of Mechanical and Automation Engineering, The Chinese University of Hong Kong. X. Li is with the Department of Automation, Tsinghua University. P. Li is with the School of Mechanical Engineering and Automation, Harbin Institute of Technology (Shenzhen). This work was supported in part by the VC Fund 4930745 of the CUHK T Stone Robotics Institute, and in part by the Shenzhen and Hong Kong Joint Innovation Project under Grant no. SGLH20161209145252406. Corresponding author: X. Li (xiangli@tsinghua.edu.cn)

target, while the robotic arm can provide position, velocity information in real-time.

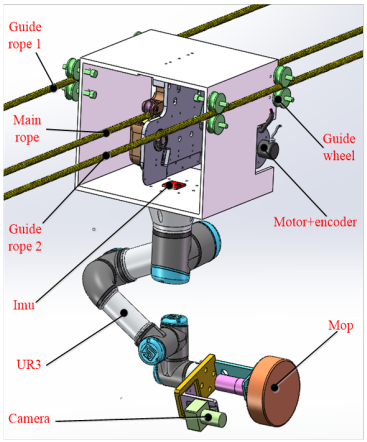

Fig. 1. 3D Model of Rope-Climbing Robot Manipulator(*RCRM*).

The working process of the *RCRM* is separated into two steps: first, the *RCR* moves to the designate horizontal position and stops; second, the robotic arm carries out the assigned task. The controlled plant of each step, which are the *RCR* and the robotic arm are mutually independent in each control step, which means only one plant is moving in each step.

The control of *RCR* along the rope is a solved problem of our previous work, seen in [10] and [19]. So the dynamic model of the single *RCR* movement along the rope is not introduced here. The main control problem in this paper is the robotic arm control in the external vibrating environment.

The control of the robotic arm part is a vision-based control problem. The *RCRM* is a floating-base system, prone to vibrate under external influences. Our purpose is to control the end effector, to the specified position under the vibration environment. Unlike the fixed base robotic arm position control, which needs 6 independent joints to get fully-actuated. The *RCRM* includes another 6 DoF for the base position except the 6 DoF of the end effector. To get the whole system fully-actuated, at least 12 independent actuators are needed, which greatly increases the weight of the system, and energy consumption. Thus, the control problem to get the whole *RCRM* work well and fine in the vibrated environment with a general 6 DoF robotic arm, and cheap and available sensors is quite a big challenge.

III. Adaptive Vision-Based Control for *RCRM*

In this section, a vision-based control scheme is proposed for *RCRM* under vibrating environment. The precise position control of the robotic manipulator in image space can be achieved even the system vibration is excited by the external factors.

A. *RCRM Kinematics*

As show in Fig. 2, a camera is fixed on UR3 robot end effector. Five coordinate frames are induced in the expression, the base frame $\{O_b\}$, the end-effect frame $\{E\}$,

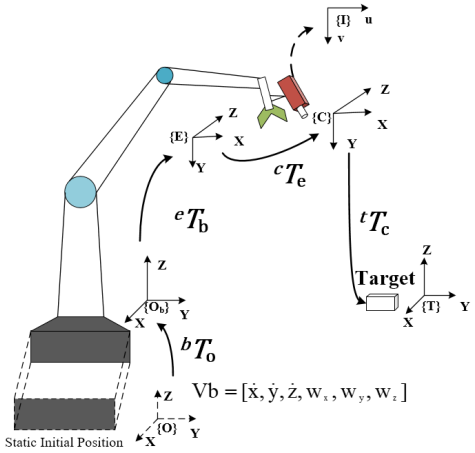

Fig. 2. Frame Declaration of *RCRM*.

$\{O\}$ is the base frame at the static equilibrium point, while $\{O_b\}$ is the real-time coordinate system during the motion movement of the mechanical platform. Homogeneous matrix ${}^{b}\boldsymbol{T_o}$, which can be measured from IMU, used for representing the relationship of $\{O\}$ and $\{O_b\}$. Similarly, the relationship between $\{O_b\}$ and $\{E\}$ can be represent by a homogeneous matrix ${}^{b}\boldsymbol{T_e}$. The $\{C\}$ and $\{T\}$ are defined for RGB camera and target frame, respectively. Homogeneous matrix X [20] represents the relationships of $\{C\}$ and $\{E\}$. Image coordinate $\{I\}$ is mainly used to obtain the image coordinates of the targets.Then,according to the image Jacobian matrix $\boldsymbol{J}_p \in \Re^{2n*6}$, n is the feature number. The speed of the camera can be calculated according to [21]:

$$\dot{\boldsymbol{P}} = \boldsymbol{J}_p * \boldsymbol{V}_c \tag{1}$$

where $\dot{\boldsymbol{P}}$ is feature speed in the frame $\{I\}$, $\boldsymbol{J}_p \in \Re^{2n*6}$, n is the feature number $\boldsymbol{V}_c$ is the camera speed in the frame $\{E\}$.

In order to drive the UR3 arm towards a designate feature point in image space, linear controller is used [21]:

$$\dot{\boldsymbol{P}} = \lambda * (\boldsymbol{P}^* - \boldsymbol{P}), \tag{2}$$

where $\boldsymbol{P}^* - \boldsymbol{P}$ is the pixel error between the feature point to designate point. Through this control law, the exponential convergence in the image space can be guaranteed. Substituting eq. 1, into eq. 2, we can have

$$\boldsymbol{V_c} = \boldsymbol{J_p^+} * \dot{\boldsymbol{P}}, \tag{3}$$

where $\boldsymbol{J_p^+}$ represent the pseudo-inverse for image Jacobian $\boldsymbol{J_p}$.

With the transfer relation of camera and end effector, the designed end effector speed can be calculated.

$$\boldsymbol{V_e} = {}^{e}\boldsymbol{J_c^{-1}} * \boldsymbol{V_c}, \tag{4}$$

where the ${}^{e}\boldsymbol{J_c}$ can be calculated by:

$${}^{e}\boldsymbol{J_c} = \boldsymbol{J_v}({}^{c}\boldsymbol{T_e}) = \begin{bmatrix} {}^{e}\boldsymbol{R_c} & -{}^{e}\boldsymbol{R_c} * Skew({}^{c}\boldsymbol{T_e}) \\ \boldsymbol{0}_{3\times3} & {}^{e}\boldsymbol{R_c} \end{bmatrix}, \tag{5}$$

If the robotic arm base is fixed, through robotic arm Jacobian, we can transfer the end effector speed to the joint space. However, for the floating base, the velocity of the base will influence the end effector speed and the camera speed. So, the designed end effector speed $\boldsymbol{V_{ed}}$ should consider the influence of the base velocity $\boldsymbol{V_b}$, which can be calculated by:

$$\boldsymbol{V_{ed}} = \boldsymbol{V_e} - {}^{e}\boldsymbol{J_b} * \boldsymbol{V_b}, \tag{6}$$

The calculation of the base and end effector Jacobian ${}^{e}\boldsymbol{J_b}$ can also be obtained through the method of eq. 5.

Then, UR3 homogeneous matrix ${}^{b}\boldsymbol{T_e}$ is applied to calculate joint velocity to joint space:

$$\dot{\boldsymbol{q}} = \boldsymbol{J}^{\dagger} * \boldsymbol{V_{ed}}, \tag{7}$$

where $\boldsymbol{V_j}$ is the joint velocity, $\boldsymbol{J}^{\dagger}$ is the pseudo-inverse of the robot Jacobian. For the floating base, the velocity of the base will influence the end effector speed and the camera speed. At last, after all the above calculations, the camera can be derived to the desired feature point.

B. RCRM Dynamics

To model dynamics of the system, we make the following assumptions:

Assumption 1: *The rope is sufficiently long and the mass on the rope is homogenously distributed. Furthermore, the rope is always in tension so that the modulus and other physical characteristics of the rope remain unchanged during the operation.*

Assumption 2: *The RCR and the robotic manipulator is excited once by the external disturbance, no different levels of vibration are imposed to the system.*

Assumption 3: *The mass and moment inertia of the RCR and the robotic manipulator is larger than the rope so that the vibration of the rope is mainly caused by the inertia forces of the robots and disturbances.*

Since the cable we use is stainless rope, with 14mm diameter, and 4 meters long, while RCR are 400mm width (detailde configuration can be refered in 19), the cable is stretched in tension when the RCR deployed on it. So the assumption 1 is reasonable. According to this, the rope physical parameters are constant. Since this paper considers the vibration suppression effects comparing with no controller deployed condition, one time pulse external interference can be direct and enough to tell the truth, differet levels of vibration are not considered here, and will be left for the future work, while assumption 3 guarantees that the external vibration can be attenuated.

Since the control target here is the vibration suppression of the robotic arm, the *RCR* is not actively driven. The wrench to robot base comes from guide rope1, rope2 and the main rope. When guide ropes only work for support the whole frame, the main wrench source is the main rope, so the wrench from the ropes, can be simplified as one rope here. The force from the rope to *RCRM* is depicted in Fig. 3. The sectional view of the stainless rope can be seen in the Fig. 3, according to the mechanical model [22] of this kind or

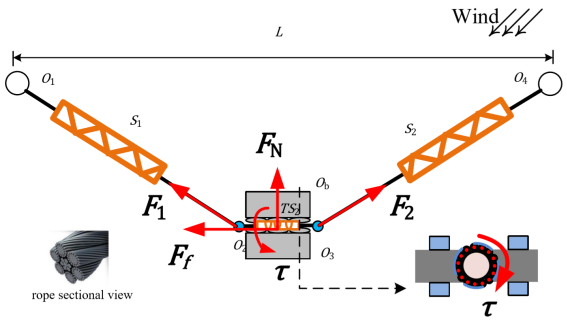

Fig. 3. Analysis of Wrench from Rope to *RCRM*.

wire rope, it can be simplified as the spring model at the longitude axis and the sectional axis, as shown in Fig. 3, the force to the robotic arm comes from the left segment rope, the force is $\boldsymbol{F_1} \in \Re^3$, and the right segment rope, whose force is $\boldsymbol{F_2} \in \Re^3$, also there is friction between the rope and the base $\boldsymbol{F_f} \in \Re^3$ and the normal force $\boldsymbol{F_N} \in \Re^3$, as we can not clearly defined the direction, it is not shown in the Fig. 3. Due to related rotation angle of the left segment and right segment, the rope is twisted by the robotic arm base, which will give a twisted torque $\boldsymbol{\tau_b} \in \Re^3$ to the robotic arm base oppositely, also the circumferential direction friction torque $\boldsymbol{\tau_f} \in \Re^3$ should be considered. Since these force and torque are all linear to the base displacement, they can be simplified as the following equations:

$$\boldsymbol{F_1} + \boldsymbol{F_2} + \boldsymbol{F_f} + \boldsymbol{F_N} = \boldsymbol{F_b} = \boldsymbol{K_x}\boldsymbol{X} + \boldsymbol{C_x}\dot{\boldsymbol{X}} \tag{8}$$

$$\boldsymbol{\tau_b} = \boldsymbol{\tau} + \boldsymbol{\tau_f} = (\boldsymbol{K_\theta}\boldsymbol{\theta} + \boldsymbol{C_\theta}\dot{\boldsymbol{\theta}})\boldsymbol{d} = \boldsymbol{K_\tau}\boldsymbol{\theta} + \boldsymbol{C_\tau}\dot{\boldsymbol{\theta}} \tag{9}$$

where, $\boldsymbol{F_b} \in \Re^3$ is the resultant of $\boldsymbol{F_1}$, $\boldsymbol{F_2}$, $\boldsymbol{F_N}$ and $\boldsymbol{F_f}$, to simplified, we can regard the base force as a linear spring damper system; while $\boldsymbol{\tau_b} \in \Re^3$ is the resultant of the $\boldsymbol{\tau}$ and the torque $\boldsymbol{\tau_f}$, which comes from all forces, still, the torque is simplified as a twist spring damper system; d is the diameter of the rope, $\boldsymbol{K_x} = \mathrm{diag}(K_1, \cdots, K_3) \in \Re^{3\times3}$ and $\boldsymbol{K_\tau} = \mathrm{diag}(K_{\tau1}, \cdots, K_{\tau3}) \in \Re^{3\times3}$ are the equivalent linear spring and twisted spring stiffness [15]; $\boldsymbol{C_x} = \mathrm{diag}(C_1, \cdots, C_3) \in \Re^{3\times3}$ and $\boldsymbol{C_\tau} = \mathrm{diag}(C_{\tau1}, \cdots, C_{\tau3}) \in \Re^{3\times3}$ are the equivalent linear damper and twisted damper. $\boldsymbol{X}$ and $\boldsymbol{\theta}$ are the position and attitude related to the initial static equilibrium point, respectively.

The whole *RCRM* consists of two subsystems: robotic arm and RCR. While the rope cannot be actively controlled and RCR is not activated, the dynamic model only contains the robotic arm, which can be described:

$$\begin{aligned} \boldsymbol{M}(\boldsymbol{X},\boldsymbol{\theta},\boldsymbol{q})\ddot{\boldsymbol{q}} + \boldsymbol{C}(\dot{\boldsymbol{X}},\boldsymbol{X},\dot{\boldsymbol{\theta}},\boldsymbol{\theta},\dot{\boldsymbol{q}},\boldsymbol{q})\dot{\boldsymbol{q}} + \boldsymbol{G}(\boldsymbol{X},\boldsymbol{\theta},\boldsymbol{q}) \\ = \boldsymbol{\tau} + \boldsymbol{J_R^T}\boldsymbol{F_b} + \boldsymbol{\tau_b}, \end{aligned} \tag{10}$$

Substituting eq. 9 into eq. 10, we can have

$$\begin{aligned}\boldsymbol{M}(\boldsymbol{X},\boldsymbol{\theta},\boldsymbol{q})\ddot{\boldsymbol{q}}+\boldsymbol{C}(\dot{\boldsymbol{X}},\boldsymbol{X},\dot{\boldsymbol{\theta}},\boldsymbol{\theta},\dot{\boldsymbol{q}},\boldsymbol{q})\dot{\boldsymbol{q}}+\boldsymbol{G}(\boldsymbol{X},\boldsymbol{\theta},\boldsymbol{q})\\ =\boldsymbol{\tau}+\boldsymbol{J}_{\boldsymbol{R}}^{T}(\boldsymbol{K}_{\boldsymbol{x}}\boldsymbol{X}+\boldsymbol{C}_{\boldsymbol{x}}\dot{\boldsymbol{X}})+\boldsymbol{K}_{\boldsymbol{\tau}}\boldsymbol{\theta}+\boldsymbol{C}_{\boldsymbol{\tau}}\dot{\boldsymbol{\theta}},\end{aligned}\tag{11}$$

where $\boldsymbol{q}=[q_1,\cdots,q_n]^T\in\Re^n$ is the robotic arm joint angle and n is the joint number of the robotic arm, q_i $(i=1,\cdots,n)$ is the joint angle of the i^{th} robot joint; $\boldsymbol{M}(\boldsymbol{X},\boldsymbol{\theta},\boldsymbol{q})\in\Re^{n\times n}$ is the inertia/mass, where elements in $\boldsymbol{M}$ are related to the base position and attitude; $\boldsymbol{C}(\dot{\boldsymbol{X}},\boldsymbol{X},\dot{\boldsymbol{\theta}},\boldsymbol{\theta},\dot{\boldsymbol{q}},\boldsymbol{q})\dot{\boldsymbol{q}}\in\Re^{n\times n}$ denotes the centripetal and Coriolis torque/force, and $\boldsymbol{G}(\boldsymbol{X},\boldsymbol{\theta},\boldsymbol{q})\in\Re^n$ is the gravity matrix; $\boldsymbol{\tau}\in\Re^n$ is the control input; $\boldsymbol{J_R}$ denotes the generalized Jacobian of the robotic arm, due to the force is exerted on the base, unlike the force exerted on the end effector, the Jacobian can be obtained as the same as the common Jacobian, but at this time, the robotic arm configuration is the reverse of the robotic arm, in which base is regarded as end effector while end effector as base.

Equation (11) describes the dynamic model of *RCRM*. According to assumption 1, the rope physical parameters $\boldsymbol{K_x}$, $\boldsymbol{C_x}$, $\boldsymbol{K_\tau}$, $\boldsymbol{C_\tau}$ are all constant. So that the rope to manipulator wrench $\boldsymbol{F_b}$ and $\boldsymbol{\tau_b}$ can be linearized with respect to $\boldsymbol{X}$ and $\boldsymbol{\theta}$, while the base position and attitude $\boldsymbol{X}$ and $\boldsymbol{\theta}$ can be obtained through sensors and $\boldsymbol{J^T}$ can be calculated with the robotic arm joint position in real time.

In the robot dynamic model eq. 10, according to the model in [17], the dynamic parameters $\boldsymbol{M}$, $\boldsymbol{C}$, $\boldsymbol{G}$ are bounded; The inertia/mass matrix $\boldsymbol{M}$ is symmetric and positive definite; The matrix $\dot{\boldsymbol{M}}-2\boldsymbol{C}$ is skew-symmetric; What's more, the left side of Eq. 11 can be parameterized as the regressor form:

$$\begin{aligned}\boldsymbol{M}(\boldsymbol{X},\boldsymbol{\theta},\boldsymbol{q})\ddot{\boldsymbol{q}}+\boldsymbol{C}(\dot{\boldsymbol{X}},\boldsymbol{X},\dot{\boldsymbol{\theta}},\boldsymbol{\theta},\dot{\boldsymbol{q}},\boldsymbol{q})\dot{\boldsymbol{q}}+\boldsymbol{G}(\boldsymbol{X},\boldsymbol{\theta},\boldsymbol{q})\\ -(\boldsymbol{J}_{\boldsymbol{R}}^{T}(\boldsymbol{K}_{\boldsymbol{x}}\boldsymbol{X}+\boldsymbol{C}_{\boldsymbol{x}}\dot{\boldsymbol{X}})+\boldsymbol{K}_{\boldsymbol{\tau}}\boldsymbol{\theta}+\boldsymbol{C}_{\boldsymbol{\tau}}\dot{\boldsymbol{\theta}})\\ =\boldsymbol{Y_d}(\dot{\boldsymbol{X}},\boldsymbol{X},\dot{\boldsymbol{\theta}},\boldsymbol{\theta},\ddot{\boldsymbol{q}},\dot{\boldsymbol{q}},\boldsymbol{q})\boldsymbol{\theta_d},\end{aligned}\tag{12}$$

where $\boldsymbol{\theta_d}$ is the vector of dynamic parameters, and $\boldsymbol{Y_d}(\dot{\boldsymbol{X}},\boldsymbol{X},\dot{\boldsymbol{\theta}},\boldsymbol{\theta},\dot{\boldsymbol{q}},\boldsymbol{q})$ is the dynamic regressor matrix.

C. Adaptive Vision-Based Control

From the dynamic eq. 11, the main problem is to deal with the robotic manipulator parameter dynamics and external dynamics from the rope, from the derivation above, the robotic manipulator dynamics are $\boldsymbol{M}$, $\boldsymbol{C}$, $\boldsymbol{G}$, while the external dynamics from the rope can be simplified as $\boldsymbol{K_x}$, $\boldsymbol{C_x}$, $\boldsymbol{K_\tau}$, $\boldsymbol{C_\tau}$, which means that in the Eq. 12, the dynamic parameter vector $\boldsymbol{\theta_d}$ is unknown such that [23]

$$\begin{aligned}\boldsymbol{Y_d}(\dot{\boldsymbol{X}},\boldsymbol{X},\dot{\boldsymbol{\theta}},\boldsymbol{\theta},\ddot{\boldsymbol{q}},\dot{\boldsymbol{q}},\boldsymbol{q})\hat{\boldsymbol{\theta}_d}\\ =\hat{\boldsymbol{M}}(\boldsymbol{X},\boldsymbol{\theta},\boldsymbol{q})\ddot{\boldsymbol{q}}+\hat{\boldsymbol{C}}(\dot{\boldsymbol{X}},\boldsymbol{X},\dot{\boldsymbol{\theta}},\boldsymbol{\theta},\dot{\boldsymbol{q}},\boldsymbol{q})\dot{\boldsymbol{q}}\\ +\hat{\boldsymbol{G}}(\boldsymbol{X},\boldsymbol{\theta},\boldsymbol{q}),\\ -(\boldsymbol{J}_{\boldsymbol{R}}^{\boldsymbol{T}}(\hat{\boldsymbol{K}}_{\boldsymbol{x}}\boldsymbol{X}+\hat{\boldsymbol{C}}_{\boldsymbol{x}}\dot{\boldsymbol{X}})+\hat{\boldsymbol{K}}_{\boldsymbol{\tau}}\boldsymbol{\theta}+\hat{\boldsymbol{C}}_{\boldsymbol{\tau}}\dot{\boldsymbol{\theta}})\end{aligned}\tag{13}$$

where $\hat{\boldsymbol{\theta}_d}$ denotes the estimation of $\boldsymbol{\theta_d}$. To compensate the dynamics, first, introducing a sliding vector:

$$\boldsymbol{s}=\dot{\boldsymbol{q}}-\dot{\boldsymbol{q}}_{\boldsymbol{r}},\tag{14}$$

where $\dot{\boldsymbol{q}}_{\boldsymbol{r}}$ is a reference vector specified as:

$$\dot{\boldsymbol{q}}_{\boldsymbol{r}}=\dot{\boldsymbol{q}}_{\boldsymbol{d}}-\boldsymbol{\alpha}_s\Delta\boldsymbol{q},\tag{15}$$

Then the control term $\boldsymbol{\tau}$ is specified as:

$$\boldsymbol{\tau}=-\boldsymbol{K_s}\boldsymbol{s}+\boldsymbol{Y_d}(\dot{\boldsymbol{X}},\boldsymbol{X},\dot{\boldsymbol{\theta}},\boldsymbol{\theta},\dot{\boldsymbol{q}},\boldsymbol{q},\ddot{\boldsymbol{q}}_{\boldsymbol{r}},\dot{\boldsymbol{q}}_{\boldsymbol{r}})\hat{\boldsymbol{\theta}_d},\tag{16}$$

where $\boldsymbol{K}_s\in\Re^{n\times n}$ is positive-definite.

The update law can be used to estimate the dynamic parameters [10]:

$$\dot{\hat{\boldsymbol{\theta}}}_{\boldsymbol{d}}=-\boldsymbol{L_d}\boldsymbol{Y}_{\boldsymbol{d}}^{T}(\dot{\boldsymbol{X}},\boldsymbol{X},\dot{\boldsymbol{\theta}},\boldsymbol{\theta},\dot{\boldsymbol{q}},\boldsymbol{q},\ddot{\boldsymbol{q}}_{\boldsymbol{r}},\dot{\boldsymbol{q}}_{\boldsymbol{r}})\boldsymbol{s},\tag{17}$$

where $\boldsymbol{L_d}\in\Re^{n_d\times n_d}$ is a diagonal and positive-definite matrix.

Theorem: *The proposed controller described by eq. 16 for RCRM guarantees the stability of the closed-loop system and the convergence of tracking errors.*

Proof: To simplify the representation, in the proof part, we use $\boldsymbol{M}(\cdot)$, $\boldsymbol{C}(\cdot)$ and $\boldsymbol{Y_d}(\cdot)$ to represent $\boldsymbol{M}(\boldsymbol{X},\boldsymbol{\theta},\boldsymbol{q})$, $\boldsymbol{C}(\dot{\boldsymbol{X}},\boldsymbol{X},\dot{\boldsymbol{\theta}},\boldsymbol{\theta},\dot{\boldsymbol{q}},\boldsymbol{q})$, $\boldsymbol{Y_d}(\dot{\boldsymbol{X}},\boldsymbol{X},\dot{\boldsymbol{\theta}},\boldsymbol{\theta},\ddot{\boldsymbol{q}},\dot{\boldsymbol{q}},\boldsymbol{q})$.

Substituting eq. 13 and 17 into the dynamic model eq. 11 yields the following dynamic equation:

$$\boldsymbol{M}(\cdot)\dot{\boldsymbol{s}}+(\boldsymbol{C}(\cdot)+\boldsymbol{K_s})\boldsymbol{s}+\boldsymbol{Y_d}(\cdot)\Delta\boldsymbol{\theta_d}=\boldsymbol{0}.\tag{18}$$

A Lyapunov-like function is proposed as:

$$V=\tfrac{1}{2}\boldsymbol{s}^T\boldsymbol{M}(\cdot)\boldsymbol{s}+\tfrac{1}{2}\Delta\boldsymbol{\theta}_{\boldsymbol{d}}^T\boldsymbol{L}_{\boldsymbol{d}}^{-1}\Delta\boldsymbol{\theta_d}.\tag{19}$$

Differentiating (19) with respect to time yields

$$\dot{V}=\boldsymbol{s}^T\boldsymbol{M}(\cdot)\dot{\boldsymbol{s}}+\tfrac{1}{2}\boldsymbol{s}^T\dot{\boldsymbol{M}}(\cdot)\boldsymbol{s}-\Delta\boldsymbol{\theta}_{\boldsymbol{d}}^T\boldsymbol{L}_{\boldsymbol{d}}^{-1}\Delta\dot{\hat{\boldsymbol{\theta}}}_{\boldsymbol{d}}.\tag{20}$$

Substituting eq. 18 into eq. 20, we have

$$\begin{aligned}\dot{V}\ &=-\boldsymbol{s}^T(\tfrac{1}{2}\dot{\boldsymbol{M}}(\cdot)-\boldsymbol{C}(\cdot))\boldsymbol{s}-\boldsymbol{s}^T\boldsymbol{K_s}\boldsymbol{s}\\ &\quad+\boldsymbol{s}^T\boldsymbol{Y_d}(\cdot)\Delta\boldsymbol{\theta_d}+\Delta\boldsymbol{\theta}_{\boldsymbol{d}}^{\boldsymbol{T}}\boldsymbol{L}_{\boldsymbol{d}}^{-1}\Delta\dot{\hat{\boldsymbol{\theta}}}_{\boldsymbol{d}}.\end{aligned}\tag{21}$$

Substituting the update law (17) into eq. 21, note that $\dot{\boldsymbol{M}}(\cdot)-2\boldsymbol{C}(\cdot)$ is skew-symmetric, $\boldsymbol{s}^T(\frac{1}{2}\dot{\boldsymbol{M}}(\cdot)-\boldsymbol{C})\boldsymbol{s}=0$, then

$$\begin{aligned}\dot{V}&=-\boldsymbol{s}^T(\tfrac{1}{2}\dot{\boldsymbol{M}}(\cdot)-\boldsymbol{C}(\cdot))\boldsymbol{s}-\boldsymbol{s}^T\boldsymbol{K}_s\boldsymbol{s}\\ &=-\boldsymbol{s}^T\boldsymbol{K_s}\boldsymbol{s}.\end{aligned}\tag{22}$$

From eq. 22, $\boldsymbol{s}$ is L_2 bounded. Note that $V>0$ and $\boldsymbol{K_s}$ is positive definite, $\dot{V}\leq 0$, then V is bounded; from eq. 19, we can get $\boldsymbol{s}$ and $\Delta\boldsymbol{\theta}$ are all bounded. Then from the eq. 18, $\dot{\boldsymbol{s}}$ is bounded, so that $\boldsymbol{s}$ is continuous. According to [24], [25], $\boldsymbol{s}$ is L_2 bounded and continuous, we can have $\boldsymbol{s}\to\boldsymbol{0}$ as $t\to\infty$, according to the sliding vector definition, we can also have $\Delta q\to\boldsymbol{0}$. Therefore, the proposed controller described by eq. 16 for *RCRM* guarantees the stability of the closed-loop system and the convergence of tracking errors. ■

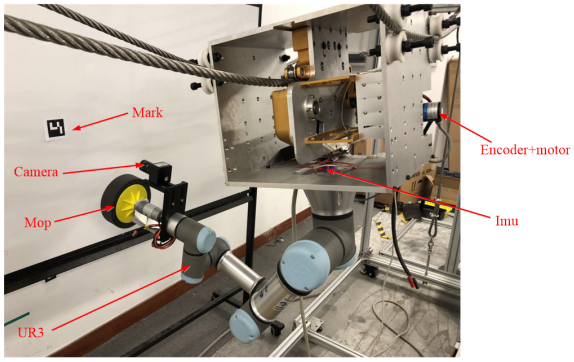

Fig. 4. Whole System of *RCRM* Experimental Setup.

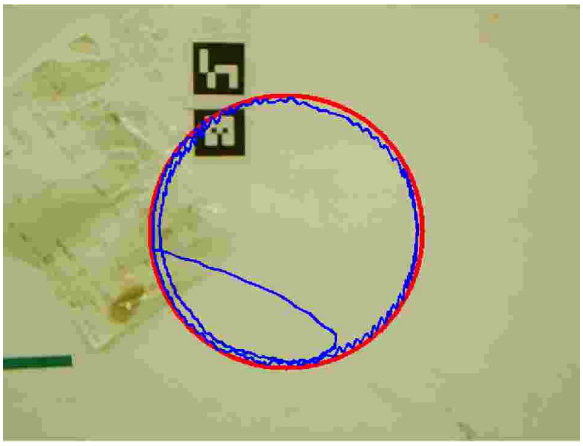

Fig. 5. Kinematic Control Result When No Vibration.

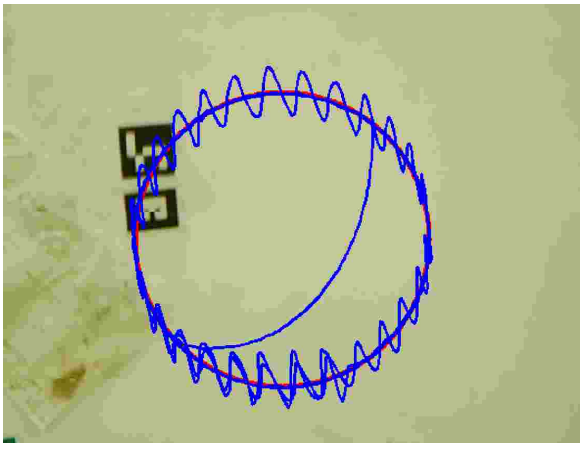

Fig. 6. Kinematic Control Result with Manual Vibration.

IV. Experiment

An experimental setup of rope climbing robot has been established in The Chinese University of Hong Kong, shown in Fig. 4, is made up with a *RCR*, a Universal Robot 3 mounted on the *RCR*; an industry camera is installed on the end effector, and it is 3 million pixels, manual lens zoom 6-12mm; a mop driven by a 12 Voltage DC motor is mounted at the end effector; an SparkFun 9DoF Razor IMU (SEN-14001) which is fixed on the UR3 mounting base, as the realization of Fig. 1. The main devices in *RCR* are, a brush DC motor with 40:1 reduction gears, which is with 250 watt rating power and 120 round per minute rating speed;a brush motor driver which can use PWM to change the motor speed, it varies from -5000 to 5000; an embedded system which here is STM32F103C8T6; and an rotary incremental optical encoder with 1200 segments which is installed at the shaft of the DC motor; a Lithium-ion Battery with 24Voltage rating voltage and 15Ampere-Hour capacity [10].

To verify the stability of proposed control scheme, the tracking experiments are used to verify the kinematic controller and the dynamic controller. Three experiments are hold here to validate the control law.

A. Kinematic Control

In the kinematic control experiment, an April tag is used as the feature point. The experiment task is to make the April tag move along the designed circle in the image space, which is a relative movement, we move the robotic arm, to fulfill the effect that the April tag is moving. The circle in image space is a 200 pixels circle around the image center. The designed image point is sent out every 0.1 second, the whole circle is combined with 500 points. The April tag is not at the first designed point, so that, the tag should chase the target trajectory, and tracking the planned trajectory. The final $\lambda = 7$, which is the variable in eq. 2, results the outcome of Fig. 5. It takes about 30 seconds to catch up with the designed trajectory.

In the following experiment, after the April tag catches up with the trajectory, we manually push the *RCR* to create an external vibration to the system. From the experiment result shown in Fig. 6, the vibration keeps existing, and never decay in the whole process, which means that the vibration coupling with the movement of robotic arm, and never calms down. It shows that the kinematic control in the vibrating environment cannot guarantee the high-accuracy operation of the manipulator since the vibration cannot be eliminated.

B. Dynamic Control When Vibration

In the dynamic control experiment, same setup as the kinematic control experiment is used, the control target is still tracking the circle in the image space. Different setting is that the dynamic controller eq. 16 is used to further decrease the influence of the external vibration by the manual push to the system. The parameter of the controller is set as: $\boldsymbol{K_s} = \boldsymbol{diag}(10, 10, 10, 10, 10, 10)$. The element of the adaptation gain in eq. 17 is set as 3. From the experiment result shown in Fig. 7, the vibration keeps existing, but decays after running 25 second, which means that the vibration coupling with the movement of the robotic arm, is controlled to calm down, which validate the performance of our dynamic controller.

V. Conclusion

This paper presents a novel *RCRM*, which provides a platform for different kinds of high-rise work. With developing the kinematic and dynamic principal of the system, a

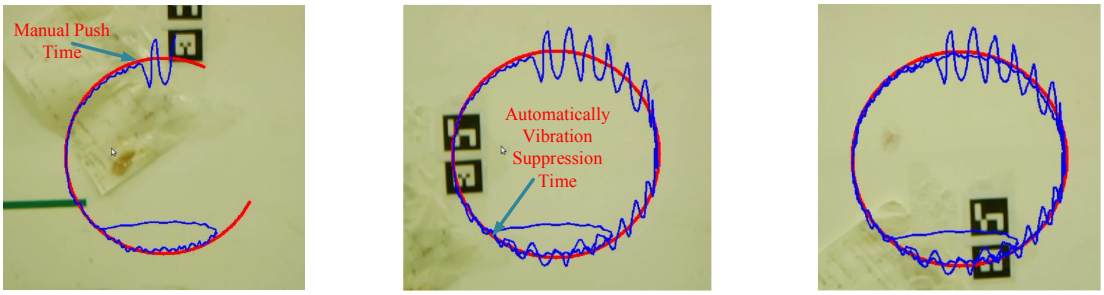

(a) (b) (c)

Fig. 7. Dynamic Control Result with Manual Vibration.

new adaptive vision-based controller is proposed for *RCRM*, which enables the robot to carry out the high-accuracy task under the unknown vibration from the rope. The proposed controller guarantees the performance of the robot in twofold. First, the control problem is directly formulated in the image space such that the exact spatial relationship between the moving base of the manipulator (due to the vibrating rope) and the target (e.g. the wall) is not required. Second, novel adaptation laws are developed to estimate the robotic manipulator parameter dynamics and external dynamics from the rope online, which is then cancelled out in the robot control input to stabilize the end effector. The controller can make the robotic arm end effector track along the designed trajectory in the image space even under the environment vibration. The stability of overall system is proved by using Lyapunov method. Two tracking experiments with manual vibration are presented to illustrate the performance of the novel robot and the proposed controller. Further research will focus on improving the efficiency of the controller, other unmodeled dynamics will be also considered.

REFERENCES

[1] L. F. Penin, R. Aracil, M. Ferre, and E. Pinto, "Telerobotic system for live power lines maintenance: Robtet," in *IEEE International Conference on Robotics and Automation, 1998. Proceedings*, pp. 2110–2115 vol.3, 1998.

[2] T. Kim, Y. Jeon, S. Yoo, K. Kim, H. S. Kim, J. Kim, T. Kim, Y. Jeon, S. Yoo, and K. Kim, "Development of a wall-climbing platform with modularized wall-cleaning units," *Automation in Construction*, vol. 83, pp. 1–18, 2017.

[3] K. H. Cho, H. M. Kim, Y. H. Jin, F. Liu, H. Moon, J. C. Koo, and H. R. Choi, "Inspection robot for hanger cable of suspension bridge: Mechanism design and analysis," *IEEE/ASME Transactions on Mechatronics*, vol. 18, no. 6, pp. 1665–1674, 2013.

[4] J. Luo, S. Xie, and Z. Gong, "Cable maintenance robot and its dynamic response moving on the horizontal cable," in *International Conference on Advanced Robotics, 2005. Icar '05. Proceedings*, pp. 514–517, 2005.

[5] F. Xu, X. Wang, and L. Wang, "Cable inspection robot for cable-stayed bridges: Design, analysis, and application," *Journal of Field Robotics*, vol. 28, no. 3, pp. 441–459, 2011.

[6] C. Balaguer, A. Gimenez, and A. Jardon, "Climbing robots mobility for inspection and maintenance of 3d complex environments," *Autonomous Robots*, vol. 18, no. 2, pp. 157–169, 2005.

[7] G. A. Lynch, J. E. Clark, P. C. Lin, and D. E. Koditschek, "A bioinspired dynamical vertical climbing robot," *International Journal of Robotics Research*, vol. 31, no. 8, pp. 974–996, 2012.

[8] L. Daler, A. Klaptocz, A. Briod, and M. Sitti, "A perching mechanism for flying robots using a fibre-based adhesive," in *IEEE International Conference on Robotics and Automation*, pp. 4433–4438, 2013.

[9] M. S. Oh and S. Jung, "Balancing and driving control of a single line play robot on the rope in the air," in *International Conference on Ubiquitous Robots and Ambient Intelligence*, pp. 107–111, 2015.

[10] G. Sun, X. Li, P. Li, Y. Meng, Z. Yang, E. Xu, and Y.-H. Liu, "A synchronization scheme for position control of multiple rope-climbing robots," in *IEEE International Conference on Robotics and Automation*, pp. 3736–3741, 2018.

[11] S. Dubowsky and E. Papadopoulos, "The kinematics, dynamics, and control of free-flying and free-floating space robotic systems," *Robotics & Automation IEEE Transactions on*, vol. 9, no. 5, pp. 531–543, 1993.

[12] D. N. Nenchev and A. Nishio, "Ankle and hip strategies for balance recovery of a biped subjected to an impact," *Robotica*, vol. 26, no. 5, pp. 643–653, 2008.

[13] D. N. Nenchev, K. Yoshida, P. Vichitkulsawat, and M. Uchiyama, "Reaction null-space control of flexible structure mounted manipulator systems," *Robotics & Automation IEEE Transactions on*, vol. 15, no. 6, pp. 1011–1023, 1999.

[14] T. Wongratanaphisan and M. O. T. Cole, "Robust impedance control of a flexible structure mounted manipulator performing contact tasks," *IEEE Transactions on Robotics*, vol. 25, no. 2, pp. 445–451, 2009.

[15] J. Ueda and T. Yoshikawa, "Robust arm configuration of manipulator mounted on flexible base," in *IEEE International Conference on Robotics and Automation, 2002. Proceedings. ICRA*, pp. 1321–1326 vol.2, 2004.

[16] X. Yang, S. S. Ge, and W. He, "Dynamic modelling and adaptive robust tracking control of a space robot with two-link flexible manipulators under unknown disturbances," *International Journal of Control*, vol. 91, no. 6, pp. 1–31, 2017.

[17] H. Wang, D. Guo, H. Xu, W. Chen, T. Liu, and K. K. Leang, "Eye-in-hand tracking control of a free-floating space manipulator," *IEEE Transactions on Aerospace & Electronic Systems*, vol. 53, no. 4, pp. 1855–1865, 2017.

[18] J. P. Alepuz, M. R. Emami, and J. Pomares, "Direct image-based visual servoing of free-floating space manipulators," *Aerospace Science & Technology*, vol. 55, pp. 1–9, 2016.

[19] G. Sun, P. Li, Y. Meng, E. Xu, Y. Zhou, and Y. Liu, "A climbing robot for inspection of lamppost in the airport: Design and preliminary experiments," in *IEEE International Conference on Robotics and Biomimetics*, pp. 436–441, 2017.

[20] F. C. Park and B. J. Martin, "Robot sensor calibration: solving ax=xb on the euclidean group," *IEEE Transactions on Robotics Automation*, vol. 10, no. 5, pp. 717–721, 2002.

[21] P. Corke, *Robotics, Vision and Control: Fundamental Algorithms In MATLAB® Second, Completely Revised*, vol. 118. Springer, 2017.

[22] W. Wu and X. Cao, "Mechanics model and its equation of wire rope based on elastic thin rod theory," *International Journal of Solids & Structures*, vol. 102, 2016.

[23] X. Li, X. Su, and Y. Liu, "Vision-based robotic manipulation of flexible pcbs," *IEEE/ASME Transactions on Mechatronics*, vol. 23, no. 6, pp. 2739–2749, 2018.

[24] J. J. Slotine, W. Li, and P. Hall, "Applied nonlinear control:united states edition," *Pearson Schweiz Ag*, 1990.

[25] S. Arimoto, *Control Theory of Nonlinear Mechanical Systems*. 1996.